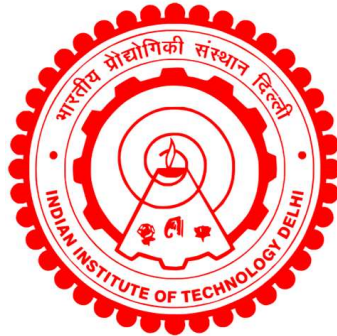


# **NEAR FIELD TERAHERTZ IMAGING AND SPECTROSCOPY**

**Uzair Aalam**



Department of Physics  
**INDIAN INSTITUTE OF TECHNOLOGY DELHI**  
July 2025

© **Indian Institute of Technology Delhi (IITD), New Delhi, 2025**

# NEAR FIELD TERAHERTZ IMAGING AND SPECTROSCOPY

*by*

**Uzair Aalam**

Department of Physics

*Submitted in fulfillment of requirements of the degree of*

**Doctor of Philosophy**

*to the*



**INDIAN INSTITUTE OF TECHNOLOGY DELHI**

**NEW DELHI 110016, INDIA**

**July 2025**

Dedicated to my parents...

## Certificate

This is to certify that the dissertation titled “**Near Field Terahertz Imaging and Spectroscopy**”, being submitted by **Uzair Aalam** to the Indian Institute of Technology Delhi, for the award of the degree of **Doctor of Philosophy**, is a record of bonafide research work carried out by him. He has worked under my guidance and supervision and has fulfilled the requirements, which to my knowledge, have reached the requisite standard for the submission of this dissertation. The results contained in this dissertation have not been submitted in part or full to any other University or Institute for the award of any degree or diploma.

Date:

**Prof. Amartya Sengupta**

Place: New Delhi

Department of Physics

Indian Institute of Technology Delhi

New Delhi, India

## Acknowledgements

First and foremost, I would like to thank my supervisor, Prof. Amartya Sengupta, for providing me with an opportunity to work in the interesting field of optics, imaging, and spectroscopy. I am appreciative of his academic supervision, patience, and support, which facilitated my exploration of various aspects of my research subject and motivated me to undertake rigorous and passionate research endeavors. I would like to express my gratitude to Dr. Aparajita Bandyopadhyay for her priceless time in extensive scientific conversations and for imparting her experience in the realm of terahertz technology, without which this work would have been much more difficult.

In addition to my supervisor, I extend my gratitude to my research committee members, Prof. Kedar B. Khare, Prof. Aloka Sinha, Prof. V. Ravishankar, and Prof. Sitikantha Roy, for their perceptive remarks, feedback, and recommendations that enhanced my research.

My sincere gratitude goes out to my colleagues, particularly Khushboo Singh for her guidance, Diksha Garg, Mayuri Kashyap, Urbi Kundu, and Puspita Chanda for their generous assistance, as well as to my friends Mohsin Ansari, Harish Khan, and Amir Khan for their constant encouragement and help throughout this arduous road.

I am incredibly grateful to my mother, father, and brother for their unwavering love, support, and patience, which have allowed me to persevere not only through my PhD but also through all of the challenging times in my life.

I cannot forget to mention the mentorship I received from my school teachers, especially Dr. Mohammad Tahir, and Mr. Vijay Pal Singh, without which I would never be where I am today.

Uzair Aalam

## Abstract

The electromagnetic waves at terahertz (THz) frequencies exhibit unique properties due to peculiar radiation-matter interaction in this frequency range. These properties of THz waves have enabled a large number of important applications both in fundamental research and industry, such as spectroscopy, the study of ultrafast phenomenon, terabit communication, non-destructive testing, biomedical diagnosis, quality control in the agri-food industry, and many more.

The applicability of THz waves has been demonstrated mostly in laboratory environments where an active control of temperature, humidity, and acoustic vibration isolation is implemented. The material to be studied is brought to the lab for analysis, which restricts the usability of THz-based studies outside such a controlled environment. Furthermore, many of the applications of THz waves involve imaging modalities for analysis. The imaging resolution, however, is inferior owing to the large wavelengths of THz range of frequencies ( $\lambda=300 \mu\text{m}$  at 1 THz). This thesis attempts to address these challenges by rigorously studying THz free-space optics and developing various optomechanical designs for THz optical devices and imaging techniques.

The thesis reports the design and development of different portable devices for THz measurements that are capable of being used for handheld operation. The presented devices have been shown to exhibit a long working distance (50 cm) for standoff sensing, wide bandwidth (up to 3.5 THz) for proximal spectroscopic sensing, along with a low weight profile and smaller footprints. Crucial applications of these devices are demonstrated in exemplary studies of hydration sensing, surface roughness measurement, interface detection in multilayered materials, and spectroscopic identification of hidden materials.

Further, the thesis also presents a THz-based imaging setup. The setup aims to utilize field confinement from a waveguide structure to construct a THz imaging system. The imaging configuration employs the near field at the output end of a hollow-core metal waveguide (HCMWG) for imaging purposes. The configuration demonstrates the ability to attain sub-wavelength resolution ( $0.8\lambda$ ) in a transmission imaging scheme. Moreover, the high-resolution capability attained by waveguide-based configuration is integrated with handheld functionality.

## सार

टेराहर्ट्ज़ आवृत्तियों पर विद्युत चुम्बकीय तरंगें इस आवृत्ति श्रेणी में विशिष्ट विकिरण-पदार्थ संपर्क के कारण अद्वितीय गुण प्रदर्शित करती हैं। टेराहर्ट्ज़ तरंगों के इन गुणों ने मौलिक अनुसंधान और उद्योग दोनों में बड़ी संख्या में महत्वपूर्ण अनुप्रयोगों को सक्षम किया है, जैसे स्पेक्ट्रोस्कोपी, अल्ट्राफास्ट घटना का अध्ययन, टेराबिट संचार, गैर-विनाशकारी परीक्षण, जैव चिकित्सा निदान, कृषि-खाद्य उद्योग में गुणवत्ता नियंत्रण, और कई अन्य। टेराहर्ट्ज़ तरंगों की प्रयोज्यता ज्यादातर प्रयोगशाला वातावरण में प्रदर्शित की गई है जहां तापमान, आर्द्रता और ध्वनिक कंपन अलगाव का सक्रिय नियंत्रण लागू किया जाता है। अध्ययन की जाने वाली सामग्री को विश्लेषण के लिए प्रयोगशाला में लाने की आवश्यकता होती है, जो ऐसे नियंत्रित वातावरण के बाहर टेराहर्ट्ज़-आधारित अध्ययनों की उपयोगिता को प्रतिबंधित करता है। इसके अलावा, टेराहर्ट्ज़ तरंगों के कई अनुप्रयोगों में विश्लेषण के लिए इमेजिंग तौर-तरीके शामिल हैं। किन्तु, इमेजिंग रिज़ॉल्यूशन टेराहर्ट्ज़ श्रेणी की आवृत्तियों की बड़ी तरंग दैर्ध्य (1 THz पर  $\lambda = 300 \mu\text{m}$ ) के कारण निम्नतर है। यह शोध प्रबंध टेराहर्ट्ज़ मुक्त-स्थान प्रकाशिकी का गहन अध्ययन करके तथा टेराहर्ट्ज़ प्रकाशिये उपकरणों और इमेजिंग तकनीकों के लिए विभिन्न प्रकाशिये-मैकेनिकल संरचना विकसित करके इन चुनौतियों का समाधान करने का प्रयास करता है।

शोध प्रबंध टेराहर्ट्ज़ माप के लिए विभिन्न चल उपकरणों की संरचना और विकास की रिपोर्ट करता है जो हाथ में पकड़कर संचालन के लिए उपयोग किए जा सकते हैं। प्रस्तुत उपकरणों में दूरस्थ-सेंसिंग के लिए लंबी कार्य दूरी (50 सेमी), समीपस्थ स्पेक्ट्रोस्कोपिक सेंसिंग के लिए विस्तृत बैंडविड्थ (3.5 THz तक), साथ ही कम वजन प्रोफाइल और छोटे फुटप्रिंट वाले उपकरण प्रदर्शित किए गए हैं। इन उपकरणों के महत्वपूर्ण अनुप्रयोगों को

हाइड्रेशन सेंसिंग, सतह खुरदरापन माप, बहुपरत सामग्री में इंटरफ़ेस का पता लगाने और छिपी हुई सामग्रियों की स्पेक्ट्रोस्कोपिक पहचान के अनुकरणीय अध्ययनों में प्रदर्शित किया गया है।

इसके अलावा, यह शोध प्रबंध एक टेराहर्ट्ज़-आधारित इमेजिंग सेटअप भी प्रस्तुत करता है। सेटअप का उद्देश्य टेराहर्ट्ज़ इमेजिंग सिस्टम का निर्माण करने के लिए वेवगाइड संरचना से फ्रील्ड कारावास का उपयोग करना है।

इमेजिंग कॉन्फ़िगरेशन इमेजिंग उद्देश्यों के लिए एक खोखले-कोर धातु वेवगाइड के आउटपुट छोर पर निकट क्षेत्र को नियोजित करता है। यह विन्यास संचरण इमेजिंग स्कीम में तरंग दैर्घ्य से नीचे के रिज़ॉल्यूशन ( $0.8\lambda$ ) प्राप्त करने की क्षमता प्रदर्शित करता है। इसके अलावा, वेवगाइड-आधारित विन्यास द्वारा प्राप्त उच्च-रिज़ॉल्यूशन क्षमताओं को हस्तचालित कार्यक्षमता के साथ एकीकृत किया गया है।

## Table of contents

<b>Certificate .....</b>	<b>i</b>
<b>Acknowledgements .....</b>	<b>ii</b>
<b>Abstract.....</b>	<b>iii</b>
<b>संक्षेप /Abstract (Hindi) .....</b>	<b>v</b>
<b>Table of contents.....</b>	<b>vii</b>
<b>List of figures.....</b>	<b>x</b>
<b>List of tables.....</b>	<b>xix</b>
<b>List of abbreviations .....</b>	<b>xx</b>
<b>1. Introduction.....</b>	<b>1</b>
1.1. Introduction to the terahertz (THz) range .....	1
1.2. Pertinence of terahertz .....	2
1.3. Attributes of THz radiation .....	3
1.4. Current challenges .....	6
1.5. Motivation and objective of this work .....	7
1.6. Overview of the thesis .....	8
1.7. Original contribution of the thesis .....	11
<b>2. Terahertz spectroscopy and imaging technique .....</b>	<b>13</b>
2.1. Introduction.....	13
2.2. Generation of broadband THz using photoconductive antenna.....	14
2.3. Detection of broadband THz using photoconductive antenna .....	17
2.4. THz time domain spectroscopy .....	19
2.5. THz imaging .....	24
<b>3. Handheld scanner head for THz-based multiparametric sensing.....</b>	<b>27</b>
3.1. Objective and motivation.....	27
3.2. The optical design of the THz scanner head .....	29
3.3. Characterization of the scanner head .....	31
3.3.1. Experimental determination of broadband performance .....	32
3.3.2. Ray trace simulation and spot diagrams .....	33

3.4. Usability of the THz scanner head in potential applications .....	37
3.4.1. Application in hydration sensing .....	37
3.4.2. Application in qualitative characterization of the surface roughness .....	42
3.4.3. Application in detecting the hidden interfaces in multilayered structures .....	45
3.5. Conclusions.....	49
<b>4. Proximal and standoff spectral sensing using handheld devices .....</b>	<b>51</b>
4.1. Objective and motivation.....	51
4.2. Design, fabrication, and characterization.....	53
4.2.1. Proximal scanner head .....	54
4.2.2. Standoff scanner head .....	57
4.3. Spectroscopic capabilities.....	61
4.4. Comparison of the scanner heads .....	63
4.5. Design improvements .....	65
4.6. Conclusions.....	68
<b>5. High-resolution THz imaging using waveguide in transmission mode.....</b>	<b>71</b>
5.1. Objective and motivation.....	71
5.2. The study of the THz response of the developed setup .....	74
5.2.1. Experimental setup.....	74
5.2.2. Experimental observations.....	76
5.3. THz imaging using the developed imaging system .....	80
5.3.1. Experimental setups for conventional and waveguide-based imaging .....	81
5.3.2. Selection of the appropriate metal waveguide .....	83
5.3.3. Attaining higher spatial resolution using HCMWG.....	88
5.3.4. Spectroscopic sensing using the developed HCMWG-based setup .....	92
5.3.5. High-resolution imaging of a leaf using the HCMWG-based setup.....	93
5.4. Conclusions.....	99
<b>6. Handheld device for high-resolution THz imaging using waveguide.....</b>	<b>101</b>
6.1. Objective and motivation.....	101
6.2. Experimental method.....	103

6.3. Results and discussion .....	105
6.3.1. Selection and characterization of waveguide.....	105
6.3.2. Frequency domain response of the doubly transmitted THz pulse .....	109
6.3.3. Imaging capabilities of the setup .....	110
6.3.4. Imaging a hidden crack using the handheld unit .....	115
6.4. Conclusions.....	117
<b>7. Miscellaneous work.....</b>	<b>119</b>
7.1. The effect of in-fill pattern of 3D printed diffractive elements on propagation of terahertz radiation .....	119
7.1.1. Introduction.....	119
7.1.2. Experimental method.....	120
7.1.3. Results and Discussion .....	121
7.1.4. Conclusions.....	123
7.2. Dehydration monitoring of agricultural products using reflection optics.....	123
7.2.1. Introduction.....	123
7.2.2. Materials and method.....	124
7.2.3. Results and discussion .....	124
7.2.4. Conclusions.....	129
<b>8. Summary, conclusions, and future scope.....</b>	<b>131</b>
8.1. Conclusions.....	131
8.2. Future directions .....	136
<b>References.....</b>	<b>139</b>
<b>Appendices.....</b>	<b>153</b>
Appendix A .....	153
Appendix B .....	157
Appendix C .....	159
Appendix D.....	161
<b>List of Publications .....</b>	<b>162</b>
<b>Bio-data.....</b>	<b>164</b>

## List of figures

Fig. no.	Caption	Page.
1.1	Different regions in the electromagnetic spectrum and the location of the THz range.	2
1.2	Characteristics of the THz range of frequencies and some of its important applications.	5
1.3	A block diagram showing a concise overview of the thesis.	10
2.1	PCA-based broadband generation of THz waves. (a) A schematic diagram showing the structure of PCA with stripline antenna structure and (b) generation of THz waves from PCA emitter due to the transient photocurrent through the photoconductor as predicted by eq. 2.3 and eq. 2.4.	17
2.2	PCA-based broadband detection of THz waves. (a) A schematic of the construction and functioning of the PCA receiver excited by a femtosecond laser pulse. The generated charge carriers experience an instantaneous electric field of THz (solid arrow in green) to constitute an electric current in the direction of the THz field. (b) A simple model of a PCA receiver consisting of two switches controlled by a femtosecond long laser pulse and a picosecond long THz pulse. The simultaneous presence of both pulses generates the signal.	18
2.3	(a) A schematic diagram of the THz TDS system. (b) The component layout of free-space part of the THz TDS system for a typical experimental setup. The THz free-space optics is generally modified depending on the study being carried out.	20

2.4	The time-resolved detection of the electric field of the THz pulse using PCA Rx by introducing a delay between the arrival of the THz pulse and the probing laser pulse using a delay line.	22
2.5	A typical signal analysis process in THz TDS measurement. (a) The recorded THz time domain signal is subjected to Fourier transformation to obtain (b) spectral amplitude and (c) spectral phase.	23
2.6	Typical optical schematics of single-pixel detector based THz imaging setups in (a) reflection configuration and (b) transmission configuration.	25
3.1	(a) The optical diagram of the THz scanner head, showing the THz emitter (Tx), THz receiver (Rx), lenses, and (b) ray tracing.	29
3.2	The visual representation of the optical experimental setup and the fully assembled portable THz scanner head, (a) and (c) depict the experimental arrangement, whereas (b) and (d) display the 3D printed THz scanner head.	30
3.3	THz time domain signal obtained from reflection measurements conducted with the THz scanner head on an aluminum metal sheet. A close-up view of the THz pulse profile is shown in the inset.	32
3.4	An examination of the frequency domain response of the THz scanner head. The operational bandwidth is limited to 2 terahertz. The pronounced spectral characteristics, marked by dashed lines, are ascribed to the absorption caused by water vapor in the environment. The accompanying phase spectrum is shown in the inset.	33
3.5	The modelled three-dimensional geometry of the optical setup.	34
3.6	The ray trace for the scanner head simulated using COMSOL. The THz source is placed at the origin (0,0).	35
3.7	The spot diagrams at different locations along the optical path of the ray.	36

3.8	The experimental setup for dehydration investigation utilizing a paper disk and portable THz scanner head. Illustration (a) depicts the damp paper on a petri dish; (b-c) display the THz scanner head positioned on the damp paper.	40
3.9	A scatter plot illustrating the relationship between the peak-to-peak amplitude of a time domain THz pulse and the acquisition time. The graph illustrates the temporal pattern of dehydration in the damp paper. The inset figure displays the time domain waveforms that were extracted experimentally and correspond to different time points.	41
3.10	The scatter graph illustrates the relationship between the peak-to-peak amplitude of the time-domain THz pulse and the acquisition time. The figure illustrates the pattern of dehydration in the cucumber slice sample. The inset image displays the time-domain waveforms that have been obtained experimentally and correspond to different time points.	42
3.11	(a) Micrographs of sandpapers 1, 2, 3, and 4, with grit numbers of 100, 220, 400, and 518 respectively, (b) the THz time-domain signal for the sandpapers. Due to intense scattering in random directions, the most rough sandpaper (sandpaper 1) exhibits the lowest THz signal.	44
3.12	(a) The specimen positioned beneath the THz scanner head and (b) layers in three-ply wood (upper) and frosted acrylic (lower).	47
3.13	Evaluation of metal, frosted acrylic, and 3-ply wood samples in the time domain. Metal exhibits a very high refractive index for THz frequencies and provides a total reflection of the THz pulse from its top surface. In contrast, acrylic and wood display 2 and 3 interfaces, respectively.	49

4.1	(a) The schematic of the optical setup utilized in the proximal scanner head, and (b) the determination of the working distance through the measurement of the angle between the incident and reflected beam.	55
4.2	(a) A snapshot of 3D design, a visual image of (b) the assembly of various modules, and (c) the complete unit of proximal scanner head.	56
4.3	The schematic of the optical setup utilized in the standoff scanner head.	57
4.4	(a) A snapshot of 3D design, a visual image of (b) the assembly of various modules, and (c) the complete unit of the standoff scanner head.	58
4.5	The characterization of scanner heads. (a) THz time domain waveform and zoomed-in THz pulse profiles (inset). (b) The THz spectral response of the scanner heads with three water vapor lines zoomed-in (inset).	60
4.6	Visual images of experimental setup using the proximal scanner head for identification of (a) the bare sample and (b) the sample behind the barrier. The red dot visible on the sample is due to the guide laser. (c) The THz spectrum of the sample exhibiting characteristic absorption peaks due to lactose at 0.54 THz and 1.35 THz.	61
4.7	Visual images of experimental setup using the standoff scanner head for identification of (a) the bare sample and (b) the sample behind the barrier. The red dot visible on the sample is due to the guide laser. (c) The THz spectrum of the sample exhibiting characteristic absorption peaks due to lactose at 0.54 THz and 1.35 THz, and spurious peaks marked by black arrows.	62
4.8	The design of the support structure for the optomechanical components used in proximal scanner head.	65

4.9	Redesigned proximal scanner head unit. (a) 3D model of the internal structure with housing and different materials used for fabrication, (b) a visual image of the scanner head unit.	67
4.10	Comparison of the metallic proximal scanner head with 3D printed scanner head. (a) The time domain waveform showing a higher peak-to-peak amplitude and (b) higher peak dynamic range for metallic unit.	67
5.1	The schematics of the experimental setups used to study the behaviour of the setup in broadband THz waves with (a) waveguide and (b) metallic aperture. (c) A photograph of the setup.	75
5.2	THz time domain waveforms recorded at each position of the lens L2.	77
5.3	The axial distribution of peak-to-peak amplitude as a function of the distance of the collecting lens from the output end of the HCMWG.	77
5.4	Peak fitted with the peak-to-peak amplitude distribution. The experimental data fits well with the Lorentzian peak with R-squared = 0.988. Solid squares: Experimental data points; solid lines: fitted data.	78
5.5	The axial distribution of peak-to-peak amplitude of THz time domain waveform as a function of the distance of collecting lens from the output end of the metallic apertures of diameters (a) 3.0 mm, (b) 2.5 mm, (c) 2.0 mm, (d) 1.5 mm, (e) 0.9 mm, (f) 0.3 mm.	79
5.6	Full width at half maximum of the axial field distribution peaks as a function of the aperture diameter.	79
5.7	Optical schematics of (a) the conventional lens-based confocal THz imaging setup and (b) the HCMWG-based imaging setup. Here, $F_x$ represents the focal length of element $x$ , and $d$ is the distance between the HCMWG output end and the sample.	82

5.8	(a) A visual representation of the experimental setup, (b) a close-up view of the HCMWG nearing the sample, (c) the HCMWG and sample observed through a microscope, and (d) a micrograph of the HCMWG cross section.	83
5.9	(a) The time-domain waveform of the transmitted signal through HCMWGs of various diameters (length: 8 cm) with vertical offset; inset (I) shows the incident THz pulse, and inset (II) provides a zoomed-in view of the time-domain waveform for the HCMWG with a diameter of 0.3 mm. (b) The peak-to-peak amplitude of the time-domain signal as a function of the diameter, fitted using eq. 5.1.	84
5.10	(a) Frequency domain response of the transmitted signal through HCMWGs with varying diameters and a length of 8 cm, (b) simulated mode profile at 1.0 THz for an HCMWG with a diameter of 0.3 mm, (c) time domain response, and (d) frequency domain response of an HCMWG with a diameter of 0.3 mm and a length of 4 cm.	86
5.11	(a) Microscopic image of the slit, (b-c) hyperspectral images of the slit obtained using the conventional confocal lens-based setup and the HCMWG-based setup, respectively. (d) Zoomed-in view of image shown in (c).	89
5.12	The field distribution across the slit, fitted with a Gaussian function for (a) the conventional imaging setup and (b) HCMWG-based setup.	90
5.13	The FWHM of the Gaussian curves fitted to the images of the slits of various widths and (b) the variation in the measured slit size across different widths.	91
5.14	THz frequency spectrum of Maltose recorded using (a) the conventional confocal lens-based setup and (b) the HCMWG-based setup, along with the corresponding absorption spectra (c) and (d). The solid arrows mark the characteristic absorption peaks of Maltose near 1.08 THz and 1.57 THz.	93

5.15	(a) A microscopic image of the sample illustrating the spot dimensions, (b) a visual photograph of the HCMWG scanning the sample, (c) a microscopic image of the leaf sample highlighting the imaged region (outlined with a black dashed rectangle) and some of the features (circled with yellow dashed lines) that have been resolved in the THz image; the THz hyperspectral images acquired using (d) the conventional confocal lens based system and I the HCMWG-based system; (f) the size measurement of the spot in the THz image along the line indicated in I.	94
5.16	(a) The sharpness of the cutoff (upper panel) and the dynamic range (lower panel) of the HCMWG based imaging setup, (b-e) THz frequency domain images at different frequencies, (f) the spectral amplitude distribution and Gaussian-fitted peak along the line indicated in I.	97
6.1	The schematics of the THz optical setups in reflection configuration for (a) traditional and (b) waveguide-based measurement setups.	103
6.2	A photograph of the experimental setup showing the placement of different components.	105
6.3	(a) THz time domain waveform of the input and transmitted signal through the waveguides of different lengths, (b) power contained in each time domain signal, (c) the propagation loss, and (d) the simulated mode profile of the dominant mode (TE <sub>11</sub> ) propagating the through the waveguide.	106
6.4	The THz time domain waveform of the signal recorded through the waveguide after double transmission.	108
6.5	The THz (a) time domain and (b) frequency domain response of the waveguide-based setup.	109

6.6	The slit images acquired using the (a) traditional configuration of THz imaging and (b) waveguide based imaging setups. (c) and (d) show the quantitative determination of slit width. A slit width of 500 $\mu\text{m}$ is calculated to be (c) 1200 $\mu\text{m}$ using the traditional imaging setup and (d) 800 $\mu\text{m}$ using the waveguide-based setup.	111
6.7	The THz (a-b) time domain images of the slit and corresponding (c-d) time-of-flight images using the traditional and waveguide-based setup, respectively. (e-f) show the scatter plot of the time delay across the image.	113
6.8	Schematic showing the tilting of the sample with respect to the optical axis of the traditional imaging setup.	114
6.9	(a) A 3D model and (b) a visual image of the handheld unit.	115
6.10	(a) Visual image of slit: bare (upper) and hidden beneath paper (lower) to emulate a hidden crack. (b) A THz time domain image of the hidden crack using the fabricated device. (c) The quantitative determination of the hidden crack dimensions.	116
7.1	(a) A photograph of FZP; (b) a photograph of 3D printed disk and its internal in-fill pattern.	121
7.2	(a) The spectral response of disk with 100% and 15% in-fill; (b-d) spectral response of disk/FZP with change in in-fill percentage and modulation of peak height with rotation.	122
7.3	Scatter plot of the peak-to-peak amplitude of the THz waveform against the time for the potato slices. The inset shows the visual image of the experimental setup in transmission mode.	125
7.4	THz time domain waveform of the transmitted signal through the potato slice sample.	126

7.5	(a) The time domain waveform of the reflected THz signal; (b) the trend of the peak amplitude with time; (c) frequency domain spectrum; and (d) visual image of the experimental setup.	127
7.6	The dehydration study of carrot slices using the reflection-based THz setup.	128
8.1	The graphical summary of the thesis. The left lobe presents high-resolution imaging using hollow core metal waveguides, the right lobe presents various handheld devices developed, and the central lobe shows the combination of high-resolution with handheld operation.	135
A1	Foot print of the device.	155
A2	Photograph of all the components of the scanner head.	155
A3	Antenna mount.	156
A4	Lens mount.	156
A5	Objective lens mount.	157
A6	Housing unit.	157
C1	A depiction of the cross section of a Gaussian beam. The $I$ is the intensity at the beam axis.	161
C2	The experimental data points fitted with the eq. C6.	162
D1	Geometric construction to show the relationship between wedge angle ( $\angle x$ ) and tilt angle ( $\angle z$ ).	163

### List of tables

3.1	Grit numbers of the selected sandpapers and their THz reflectivity.	44
4.1	Comparison of the specifications of the proximal scanner head and standoff scanner head.	64
4.2	The comparison of the metallic proximal scanner head with 3D printed plastic unit.	68
B1	material and parameters for fabrication process.	159
B2	Comparison of the presented handheld scanner with state-of-the-art handheld devices.	159

### List of abbreviations

1.	THz	Terahertz
2.	FTIR	Fourier transform infrared
3.	VISS	Visible spectroscopy
4.	STM	Scanning tunneling microscopy
5.	CW	Continuous Wave
6.	HEM	High electron mobility
7.	QCL	Quantum cascade laser
8.	UTC PD	Uni-Traveling-Carrier Photodiode
9.	PCA	Photoconductive antenna
10.	DC	Direct current
11.	TDS	Time domain spectroscopy
12.	Tx	Emitter
13.	Rx	Receiver
14.	fs	Femtosecond
15.	FFT	Fast Fourier transform
16.	IR	Infrared
17.	ToF	Time-of-flight
18.	OAPM	Off-axis parabolic mirror
19.	3D	Three dimensional
20.	SOTA	State-of-the-art
21.	PLA	Poly lactic acid
22.	ps	Picosecond
23.	EFL	Effective focal length

24.	RMS	Root-mean-squared
25.	V2X	Vehicle-to-everything
26.	CAD	Computer-aided design
27.	RFL	Reflective focal length
28.	WG	Waveguide
29.	HCMWG	Hollow-core metal waveguide
30.	s-SNOM	scattering-type scanning near-field optical microscopy
31.	FWHM	Full-width at half maximum
32.	SNR	Signal-to-noise ratio
33.	HRFZ-Si	High resistivity float zone silicon
34.	HDPE	High density polyethylene
35.	FZP	Fresnel zone plate
36.	FDM	Fused deposition modeling